International Journal of Automotive Technology, Vol. 5, No. 1, pp. 33–46 (2004)

1229-9138/2004/015-05

DEVELOPMENT OF FINITE ELEMENT HUMAN NECK MODEL FOR VEHICLE SAFETY SIMULATION

I.-H. LEE[1)*], H.-Y. CHOI[2)], J.-H. LEE[3)] and D.-C. HAN[4)]

[1)]Hankook ESI, 6F Worldwideweb Building, Kayang-dong, Kangseo-gu, Seoul 157-200, Korea
[2)]Department of Mechanical Engineering, Hongik University, Seoul 121-791, Korea
[3)]IPS International, 6F Worldwideweb Building, Kayang-dong, Kangseo-gu, Seoul 157-200, Korea
[4)]School of Mechanical and Aerospace Engineering, Seoul National Univeristy, Seoul 151-742, Korea

(Received 28 August 2003; Revised 19 December 2003)

ABSTRACT–A finite element model development of a 50th percentile male cervical spine is presented in this paper. The model consists of rigid, geometrically accurate vertebrae held together with deformable intervertibral disks, facet joints, and ligaments modeled as a series of nonlinear springs. These deformable structures were rigorously tuned, through failure, to mimic existing experimental data; first as functional unit characterizations at three cervical levels and then as a fully assembled c-spine using the experimental data from Duke University and other data in the NHTSA database. After obtaining satisfactory validation of the performance of the assembled ligamentous cervical spine against available experimental data, 22 cervical muscle pairs, representing the majority of the neck's musculature, were added to the model. Hill's muscle model was utilized to generate muscle forces within the assembled cervical model. The muscle activation level was assumed to be the same for all modeled muscles and the degree of activation was set to correctly predict available human volunteer experimental data from NBDL. The validated model is intended for use as a post processor of dummy measurement within the simulated injury monitor (SIMon) concept being developed by NHTSA where measured kinematics and kinetic data obtained from a dummy during a crash test will serve as the boundary conditions to "drive" the finite element model of the neck. The post-processor will then interrogate the model to determine whether any ligament have exceeded its known failure limit. The model will allow a direct assessment of potential injury, its degree and location thus eliminating the need for global correlates such as Nij.

KEY WORDS : Finite element model, 50th percentile male cervical spine, Hill's muscle model, Muscle activation

1. INTRODUCTION

During the vehicle crash accident, occupants are usually injured due to the acceleration caused by relative motion to the vehicle and/or secondary impact to the vehicle interior parts. Many kinds of researches have been performed to reduce such crash injuries and their results are proposed as the formats of regulation to secure the minimum safety requirements of vehicle (Lee, 2000). Within the crash safety regulations, dummies which had been designed to represent the behavior and characteristics of standard occupants are employed to assess the occupant injury.

However, these dummies are not yet applicable to the general crash directions but they rather cater to particular impact directions such as front, lateral and rear.

Besides, there is a drawback of current dummies that their designs were made mostly together with the safety regulations so they are lack of capacities to predict recently issued injury patterns.

To overcome these problems, live human volunteers and cadavers are often used but they have still limited features to represent real crash injuries. Accordingly, there is a pressing demand for an anatomic human model that can replace mechanical dummies in order to gain insight into the damage mechanisms and help establish tolerance limits for crash injuries.

Neck injury among other crash injuries occurs due to the abrupt relative motions between head and thorax rather than from direct impact loadings on the neck region. Then, soft tissues such as ligaments and muscles in the human cervical spine are easily injured when their connected bony parts have excessive relative motions to each other. The causes of whiplash injury, for example, are known to be related to the damages of soft tissues located between the adjacent vertebrae that experience extraordinary movements to each other.

These understanding of basic injury mechanisms of

*Corresponding author. e-mail: lih@esi.co.kr

human neck, however, are quite limited to some extent and many studies are under going both experimentally (Bandak, 1996; Szabo, 1996; Donnelly, 1997; Nahum, 1997; van der Horst, 1997; Ono, 1999) and analytically (Bandak, 1994; Voo, 1996; Claessens, 1997; Willinger, 1999; Choi, 1999). Recently numerical simulations, especially using the finite element method, have been utilized to investigate the hypothetical theories based on experiments and clinical findings. Therefore, it becomes important task to express precise and dynamic movements of translation and rotation of cervical vertebrae to investigate the injury mechanisms by using analytical human neck model. To achieve this, human body components such as hard tissue (i.e. skeleton), soft tissue (i.e. ligament, muscle, flesh and etc.) and organs should be modeled anatomically in detail. And the physiological and mechanical properties of each component also need to be assigned precisely.

The paper first deals with the finite element modeling of the human neck. For this purpose, the model aspects of the cervical vertebrae, the inter-vertebral discs, the cervical spine ligaments, the neck muscles and the head/neck skin models are described. The paper then deals with the validation of the model by establishing calibrated tensile and bending responses for selected functional cervical spine units; correct tensile responses for the whole cervical spine; validated responses to NBDL volunteer frontal tests. The results demonstrate the validity of the model to be used for representing human head/neck response and assessing the potential neck injury risks during the crash events.

2. FINITE ELEMENT MODELING OF HUMAN NECK

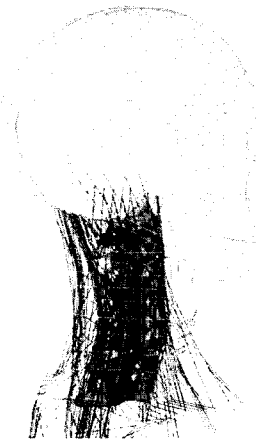

Figure 1. Finite element human neck model for SIMon program.

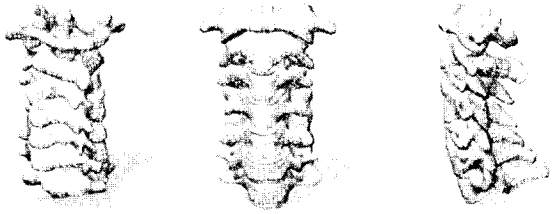

Figure 2. Three-dimensional CAD drawing of cervical spine in IGES format (www.viewpoint.com).

The model, anatomically depicted in detail, was built on 50% male geometry. The hard and soft tissues in the neck such as vertebrae, muscles, ligaments, organs, and inter-vertebral discs were modeled by using the various kinds of finite elements and material properties to represent adequate mechanical behaviors of each component. Figure 1 shows the neck model developed in this study.

2.1. Cervical Vertebrae

The geometry of the vertebrae was adopted from Viewpoint Datalab™ (VP2488: Points-11025, polygons-15726, www.viewpoint.com). Figure 2 is the corresponding 3-D CAD drawing in IGES format. In Figure 3, selected finite element models of cervical vertebrae are

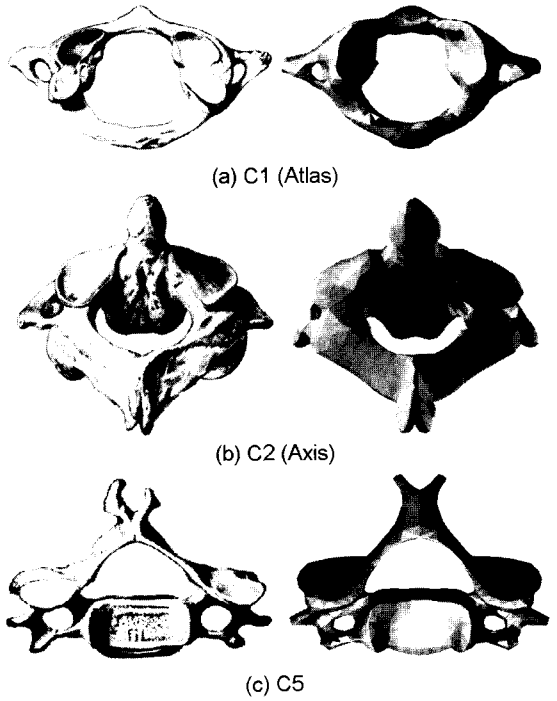

Figure 3. Cervical vertebrae (left: Anatomical picture (Gray's Anatomy), right: FE model).

Table 1. Mass and inertia properties of cervical vertebrae in the SIMon neck model.

Vertebra	Mass [g]	Moment of inertia [kg/mm^2]		
		I_{rr}	I_{ss}	I_{tt}
C0 (head)*	4,137	20,000	22,200	14,500
C1	220	220	220	420
C2	250	250	250	480
C3	240	240	240	465
C4	230	230	230	440
C5	230	230	230	450
C6	240	240	240	470
C7	220	220	220	430

(r, s, t represent the principal axes, front, lateral and superior directions, respectively)
*C0 value, including skull and facial bone, extracted from (Robbin, 1983) other vertebral values are from (Jager, 1996)

shown with corresponding anatomical features. Since the each vertebra bone was modeled as a rigid body, geometrical inertia characteristics such as center of gravity, mass moment of inertia and mass are required. The geometrical inertia characteristics of surrounding flesh for each segmental rigid body was also added to the those of the cervical vertebrae. Table 1 shows masses and moments of inertia extracted from the literature (Jager, 1996; Robbin, 1983).

The sliding interfaces with 0.01 frictional coefficient were defined between each pair of facet surfaces in cervical zygapophysial joint as well as between the posterior processes of adjacent vertebrae.

2.2. Inter-vertebral Discs

Each inter-vertebral disc was modeled by a 6 DOF joint element whose deformational characteristics, i.e. force-displacement and moment-rotation relationships were determined based on experimental measurements. The measurement for each directional stiffness of the cervical inter-vertebral discs had been performed by many researchers (Yoganandan, 2001; Edwards, 1999; Pintar, 1986; Moroney, 1999). The measurements of tensile and compressive stiffness of all cervical discs (Yoganandan, 2001; Pintar, 1986) and C4/5 motion segment (Edwards, 1999) were conducted. The tests on disc stiffness of five other directions than tension were also performed by Moroney *et al.* (Moroney, 1999). Figure 4 shows the comparison of tensile force-displacement relations between test results from Edwards (1999) and Pintar (1986). A straight line with 63 N/mm slope representing the averaged stiffness of the linear region from Pintar's measurements (Pintar, 1986) was shifted by 1 mm displacement on the assumption that the preload during

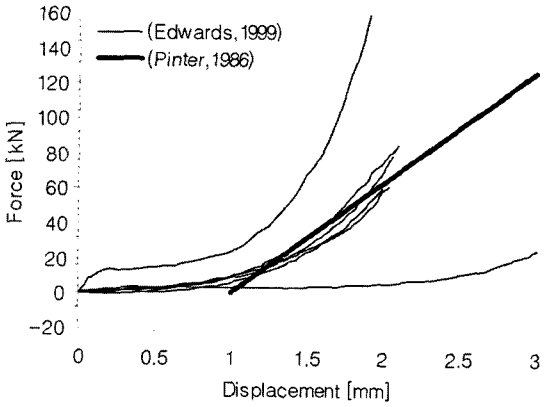

Figure 4. Tensile disc properties from literatures (Edward: C4/5 (Edwards, 1999), Pintar: averaged linear region of C2/T1 (Pintar, 1986)).

Table 2. Stiffness of cervical discs from Moroney (Moroney, 1999).

Loading mode	Stiffness*	Range
Compression [N/mm]	492 (472)	57–2060
Anterior shear [N/mm]	62 (63)	12–317
Posterior shear [N/mm]	50 (36)	13–169
Right lateral shear [N/mm]	73 (62)	17–267
Flexion [Nm/deg]	0.21 (0.14)	0.05–0.65
Extension [Nm/deg]	0.32 (0.15)	0.06–0.78
Right bending [Nm/deg]	0.33 (0.18)	0.09–0.91
CCW torsion [Nm/deg]	0.42 (0.17)	0.23–0.93

*mean values (standard deviation)

the test excluded toe region of the discs. As shown from the results of Edwards (1999) in Figure 4, the tensile stiffness would be higher at large displacement in the non-linear region and it becomes 60% more in stiffness than the average value given by Pintar.

Table 2 lists the test results of cervical disc stiffness from Moroney *et al.* (1999) which was taken from the linear region of the force-displacement curve. Therefore, the reported cervical disc stiffness from the various literatures actually represents the characteristics of the initial linear region but not for the nonlinear region with large displacements or rotations.

Accordingly, we made an assumption that these stiffness values are the average ones in the range of motion. The general schematic shape for the disc characteristics in the SIMon neck model is shown in Figure 5 and summarized in Table 3.

The third order polynomial function was adopted both in the toe zone (DN) and the range of motion (DE) while the linear line was used beyond the range of motion. The

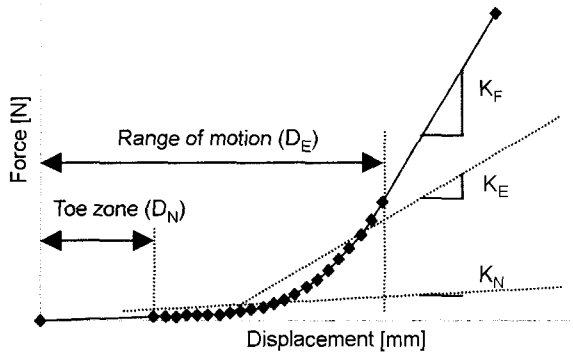

Figure 5. General schematic curve shape of disc characteristic in SIMon neck model.

Table 3. Variables in Figure 4 for cervical disc characteristics.

Variables	Reference	Remark
D_N	(Panjabi, 2001)	toe zone in cervical functional motion unit
D_E	(White, 1990)	range of motion in cervical functional motion unit
K_N	1/25 of K_E (substantially small value)	
K_E	tension from (Pintar, 1986) others from (Moroney, 1999)	linear regression of 3rd order polynomial curve fitting to the range of motion
K_F	$5 \times K_E$ for translation and $2 \times K_E$ for rotation (determined by the calibration with directional characteristics of functional motion unit)	

coefficients of the third order polynomial function were determined so that the linear regression of the range of motion becomes the value of KE which is from test measurements (Pintar 1986; Moroney 1999). Viscous damping forces of each direction were taken into account (translational damping coefficient; 300 Ns/m, rotational damping coefficient; 0.3 Nms/rad).

2.3. Ligaments

Ligaments were modeled as 1-dimensional bar elements with nonlinear force-displacement characteristics. For cruciform, transverse, and tectorial ligaments in the atlanto-axial joint however, membrane elements were used instead to allow for surface contact with the odontoid process (dens) of the axis (C2). Experimental measurements for the mechanical response of the cervical ligaments have been reported (Pintar, 1986; Yoganandan, 2001; Chazal, 1985; Edwards, 1999). Stiffness values in these literatures were abstracted and shown in Table 4. As it can be seen from Table 4, properties of all structurally important cervical ligaments were presented from Pintar (1986) and Yoganandan *et al.* (2001) but those values were fairly lower than the values proposed by Chazal (1985) and Edwards (1999). There are 5-fold differences in ALL (Anterior Longitudinal Ligament), PLL (Posterior Longitudinal Ligament) and 2.5-fold in other kinds of ligaments. The wide difference in the mechanical properties of ligaments among these tests might be due to the different test procedures of each test in specimen preparation as well as in loading and fixing of the vertebral segments. For instance, the failure of periosteum might cause slips between ligament and vertebrae, then the effective length of the ligament would increase which results in picking up less stiffness (Myers, 2003; Pintar, 2003). Also possible extra compliance and friction in the test frame could produce undesired variables in test results (Chancey, 2001; Myers, 2003).

Table 4. Cervical ligament stiffness values from literatures.

References		(Pintar, 1986)	(Yoganandan, 2001)*	(Chazal, 1985)	(Edwards, 1999)
Stiffness [N/mm]		Mean	Mean	Mean	Mean
C2-C5	ALL	16.60	16.00	71.40	
	PLL	21.40	25.40	145.40	
	LF	16.30	25.00		
	ISL	7.30	7.74		
	JC	30.70	33.60		
C5-T1	ALL	17.00	17.90		93.83
	PLL	25.90	23.00	83.70	123.73
	LF	25.30	21.60		88.05
	ISL	5.30	6.40		
	JC	29.20	36.90		74.76

*reanalyzed from Pintar's original test measurements (Pintar, 2003)

By considering these matters, magnifying factors (5 for ALL and PLL, 2.5 for other ligaments) were applied to the average stiffness values of Pintar (1986) and Yoganandan *et al.* (2001) and used in the SIMon neck model. The experimental stiffness values for the upper cervical ligament were presented by Pintar (1986) as listed in Table 5. The same scaling scheme as stated above was applied to the upper cervical ligament values in the modeling.

Chazal (1985) characterized the nonlinear force-displacement behavior of ligament with three linear parts, i.e., toe, physiological, and traumatic regions. In this study, general pattern of ligamental force-displacement

Table 5. Upper cervical ligament stiffness values from Pintar (Pintar, 1986).

Spinal level		Force [N]	Deformation [mm]	Stiffness [N/mm]
OC-C1	AA-OM	232	18.9	16.9
	PA-OM	83	18.1	5.7
	JC	320	9.9	32.6
OC-C2	TM	76	11.9	7.1
	CLV	436	12.5	19.0
	Apical	214	8.0	28.6
	Alar	357	14.1	21.2
C1-C2	ALL	263	11.8	24.0
	JC	314	9.3	32.3
	LF	111	9.6	11.6

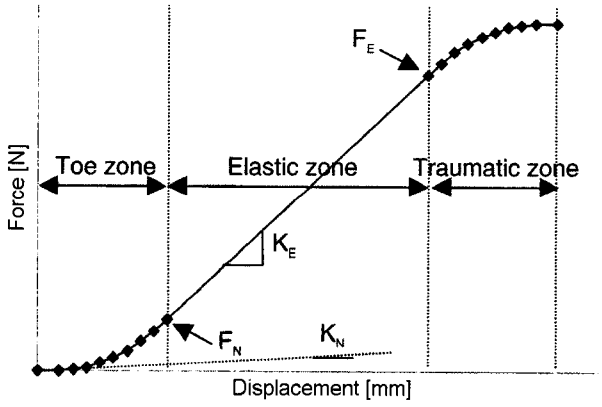

Figure 6. General pattern of ligamental force-displacement behavior.

behavior as shown in Figure 6 and Table 6 was adopted. For toe and traumatic regions in Figure 6, 3rd order polynomials functions were employed while a linear function was used for elastic zone.

As shown in Figures 7, each ligament is modeled by parallel connections of multiple single-bar elements except the upper cervical cruciform, tectorial and transverse ligaments. Thus, the reactive force existing in each ligament is a sum of forces developed by individual elements constituting that ligament. The damping effect in the ligament is modeled by viscoelastic characteristic with the damping coefficient of 150 Ns/m.

2.4. Neck Organs

The modeling of larynx in the neck located between the mandible and upper cervical vertebrae is shown in Figure 8.

During the early stage in head flexion, especially when chin was pulled directly to the rearward direction, the mandible arch begins to contact the larynx and the further flexion motion would be restricted. However the ligaments connecting the hyoid bone and thyoid and cricoid cartilages would provide some structural stiffness when the larynx bends and stretches along the cervical spine during the head extension. The hyoid bone and both

Table 6. Variables in Figure 5 for cervical ligament characteristics.

Variables	Reference	Remark
F_F	(Pintar, 1986) & (Yoganandan, 2001)	Failure load
F_E	(Chazal, 1985)	Estimated 85% of F_F
F_N	(Chazal, 1985)	Estimated 15% of F_F
K_E	(Pintar, 1986) & (Yoganandan, 2001)	Scaled 5 times for ALL/PLL and 2.5 times for other ligaments
K_N	Initial stiffness of "toe" region 1/50 of K_E (substantially small value)	

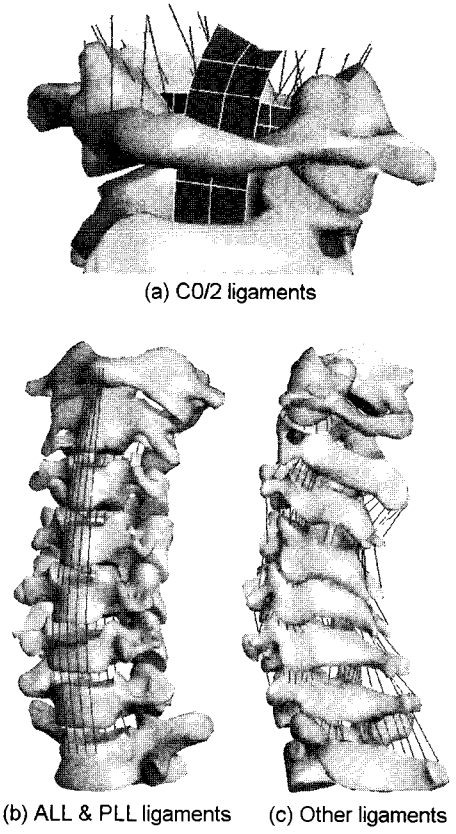

Figure 7. Ligaments in SIMon neck model.

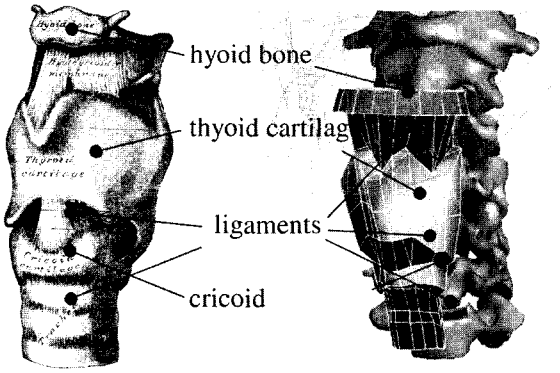

Figure 8. Larynx modeling in SIMon neck (left: Anatomical picture from Gray's Anatomy, right: FE model).

cartilages are modeled as rigid bodies and constrained respectively to nearby cervical vertebrae while the ligaments are modeled by isotropic membrane elements with 2 mm thickness and with 100 kPa elastic modulus.

2.5. Muscles

The twenty two pairs of major cervical muscles were included in the model. The geometry of each muscle is acquired from anatomy atlases (Stone, 2000) and published sources (Jager, 1996). Figure 9 shows the finite element models of the muscles and vertebrae. Muscles with broad origins or insertions were divided into multi-segments and each represented by discrete bar element(s). The muscle segments with curved geometry were formed with serially connected multi-elements of which the midway nodes were constrained to nearby vertebrae. These muscle segments with serially connected multi-elements curve around the cervical spine during the neck bending while maintain the uniform axial force transmissions. The active and passive muscle response was modeled by adopting a Hill type algorithm (ESI, 2002). The parameters for defining Hill type muscle modeling in the SIMon model are provided in Table 7.

2.6. Head and Neck Skins

The morphology of the head/neck skin for the 50% male was obtained from Robbins (Robbins, 1983). Figure 10 shows the 3-D CAD drawing of the 50% male in IGES format. Figure 11 shows the head/neck skin modeled by null shell elements with the cervical spine with and without muscles displayed.

Each cervical vertebra is linked to the surrounding skin part by using rigid body constraints. Figure 12 shows the

Table 7. Hill type muscle parameters.

Active muscle force-length properties		
Muscle fibre optimum length ratio	aL_{opt}	1.1
Shape parameter of the active muscle force-length relation	C_{sh}	0.54
Active muscle force-velocity properties		
Muscle maximum shortening velocity	aV_{max} [s^{-1}]	6
Shape parameter of the active muscle force-velocity relation during muscle shortening	C_{short}	0.2
Shape parameter of the active muscle force-velocity relation during muscle lengthening	C_{leng}	0.081
Force parameter of the active muscle force-velocity relation during muscle lengthening	C_{mvl}	1.4
Active muscle state-time properties		
Muscle activation time constant	T_a [ms]	10
Muscle deactivation time constant	T_{da} [ms]	25
Excitation time constant	T_{ne} [ms]	30
Reflex time	T_{refe} [ms]	*
Initial value of the muscle active state	A_{init}	0.01
Initial value of the excitation	E_{init}	0.01
Active muscle force properties		
Muscle fiber rest length	L_{ofib}	**
Muscle elongation at passive force equaled F_{max} as the ratio of Lofib	PE_{max}	0.6
Shape parameter of the passive muscle force-elongation relation	C_{PE}	8
Linear viscous damping coefficient of the passive muscle force	C_{damp} [Ns/m]	8

*: varies with loading condition, see the context in model validation.
**: dependent on initial location of each muscle.

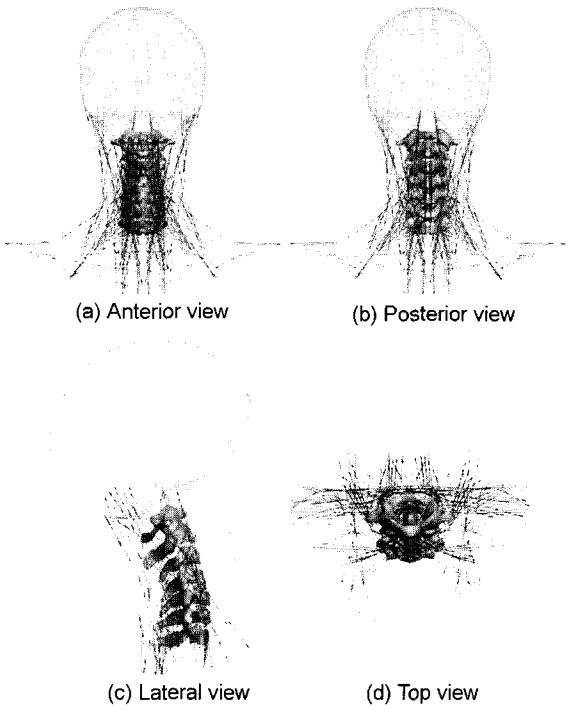

Figure 9. Muscles in SIMon neck model.

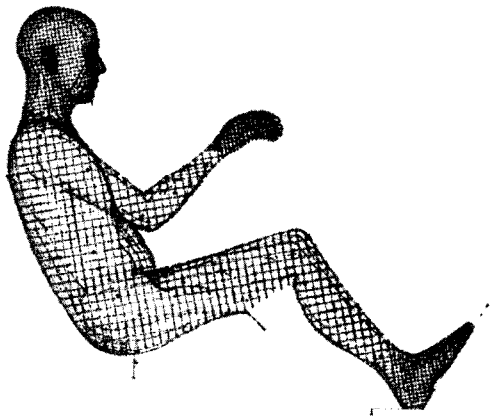

Figure 10. Three-dimensional CAD drawing of 50% male in IGES format.

nodal constraints of rigid body links between the cervical vertebrae and neck skin.

3. MODEL VALIDATION

The SIMon neck model has been validated against available experimental data. For in-intro level validation, test results with unembalmed cadaver cervical spines performed by Duke University (Chancey, 2000; Myers,

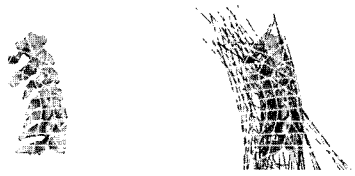

Figure 11. SIMon neck model shown with head/neck skin (right: with muscles displayed).

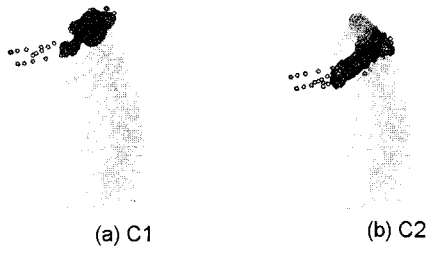

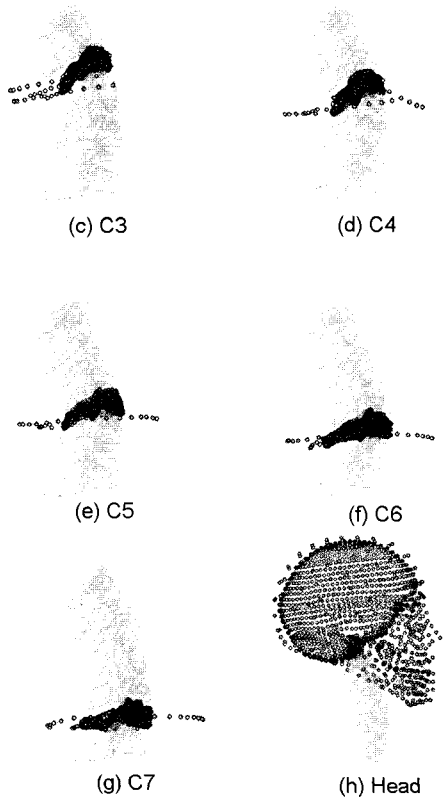

Figure 12. Rigid constraints of cervical vertebrae and neck skin (skull, mandible, and facial bone is attached to head skin).

2002; Nightingale, 2002) were utilized. The functional motion units at three cervical levels were chosen for both bending and tensile behaviors. Then, the fully assembled cervical spine under the tensile loading was simulated for the validation of overall compliance of the cervical spine. Two kinds of volunteer test were also adopted to validate the SIMon neck model with musculature effects on the head/neck response being taken into account. The validation of the SIMon neck model for the flexion, frontal sled test results of NBDL (Wismans, 1986; Thunnissen, 1995) were simulated and the JARI volunteer direct head pulling test (Ono, 2002) results were simulated for the validation of extension.

3.1. Tensile Responses for Functional Cervical Spine Units

For the validation of tensile stiffness and failure load of the SIMon neck model, test results of unembalmed human cadavers performed by Duke University (Chancey, 2000; Myers, 2001; Nightingale, 2002) were used. In the Duke test, three functional motion units, OC/C2, C4/C5 and C6/C7 were placed in a testing device designed to apply pure vertical loads. Figure 13 shows the loading and boundary conditions in the simulation which are equivalent to the test condition. As we can see from Figure 14, simulation results with the SIMon neck model correlate well with the test results.

3.2. Bending Responses for Functional Cervical Spine Units

Compliance tests of extension and flexion performed by Duke University in series with above mentioned tension tests were utilized to verify the bending characteristics of the SIMon model. In the Duke test, three functional motion units, OC/C2, C5/C6 and C7/T1 were placed in a testing device designed to apply pure bending moments.

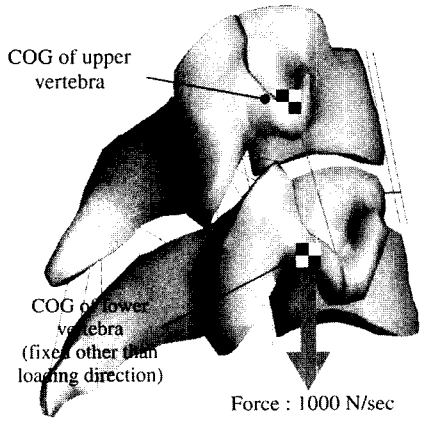

Figure 13. Tensile loading and boundary conditions for FMU simulation.

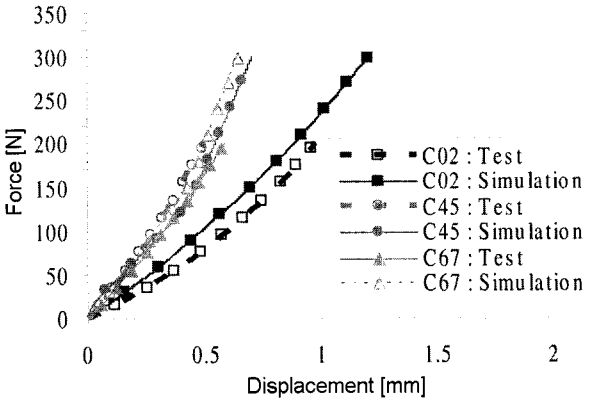

Figure 14. Comparisons of tensile force-displacement relations between Duke University cervical spine FMU test results (Nightingale, 2002) and SIMon neck simulations.

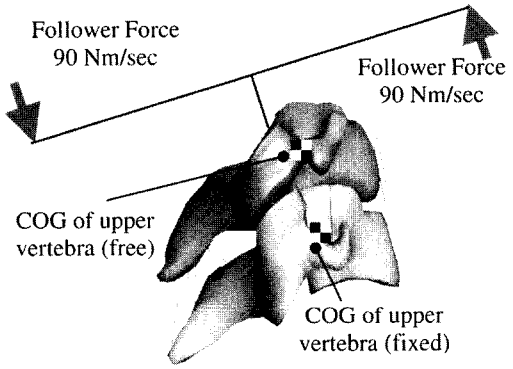

Figure 15. Bending and boundary conditions for FMU simulation.

Figure 15 shows the loading and boundary conditions in the simulation which are equivalent to the test condition. As we can see from Figure 16, simulation result with SIMon neck model correlates well with the test results for all three functional motion units.

3.3. Tensile Responses for Whole Cervical Spine

The tensile compliance of the whole cervical spine was simulated as in Figure 17 with the loading and boundary conditions equivalent to the test condition.

Under fixed-fixed end conditions in the Duke whole cervical spine tension tests, mechanical stabilization was performed using 60 cycles of a 1.0 Hz Haversine with a mean and amplitude of 75 N in tension. The actuator position was then zeroed after preconditioning. In order to take this preconditioning effect into account in the simulation, an initial tensile force with 75N was applied prior to obtain the region of force-displacement correlation as shown in Figure 18. As we can see from

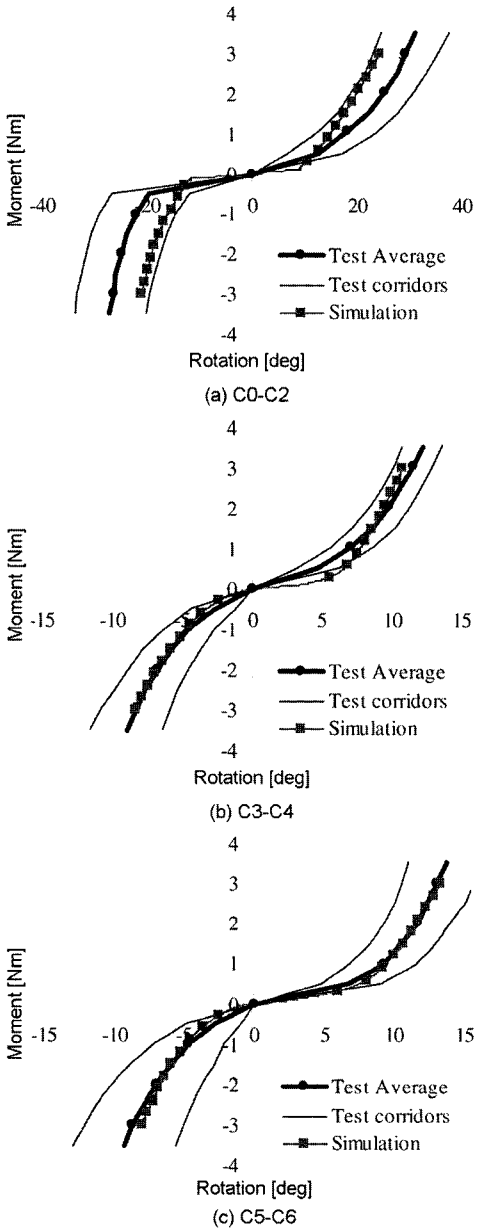

Figure 16. Comparisons of bending moment-angle relations between Duke University cervical spine FMU test results (Nightingale, 2002) and SIMon neck simulations.

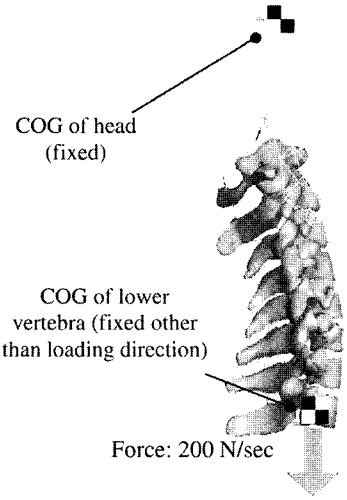

Figure 17. Tensile loading and boundary conditions for whole cervical spine simulation.

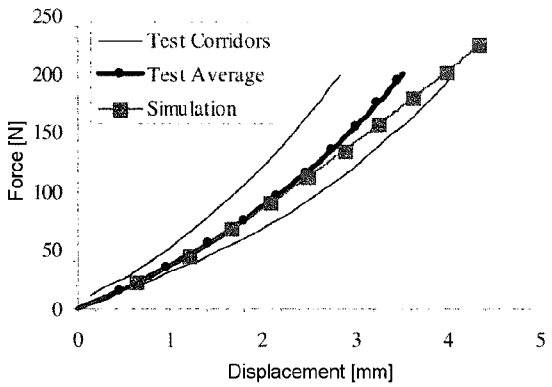

Figure 18. Comparisons of tensile force-displacement relations between Duke University cervical spine whole cervical test results (Nightingale, 2002) and SIMon neck simulations.

Figure 18, the simulation result with the SIMon neck model correlates well with the test corridors (Nightingale, 2002).

4. MUSCLE PARAMETRIC STUDY WITH NBDL VOLUNTEER FRONTAL SLED TEST

The head/neck responses of human volunteers conducted by NBDL were simulated using the neck model. Test measurements, i.e. head/neck kinematics analyzed and reported in the literature (Wismans, 1986; Thunnissen, 1995) were utilized for the simulation. Among the three kinds of NBDL test, frontal, lateral and oblique, 15G frontal sled test results were chosen to validate and for muscle parametric study. Figure 19 shows the T1 kinematic input conditions (Thunnissen, 1995) used for the simulation.

To consider the muscle activation of the human during

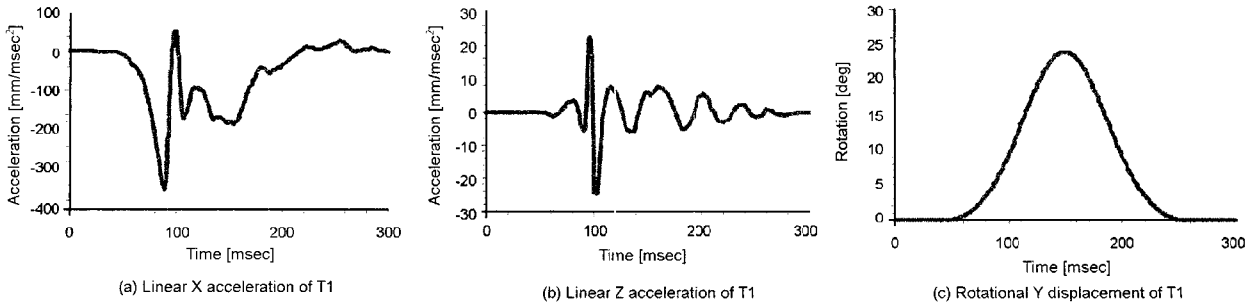

Figure 19. T1 kinematics input conditions for NBDL 15G frontal sled test.

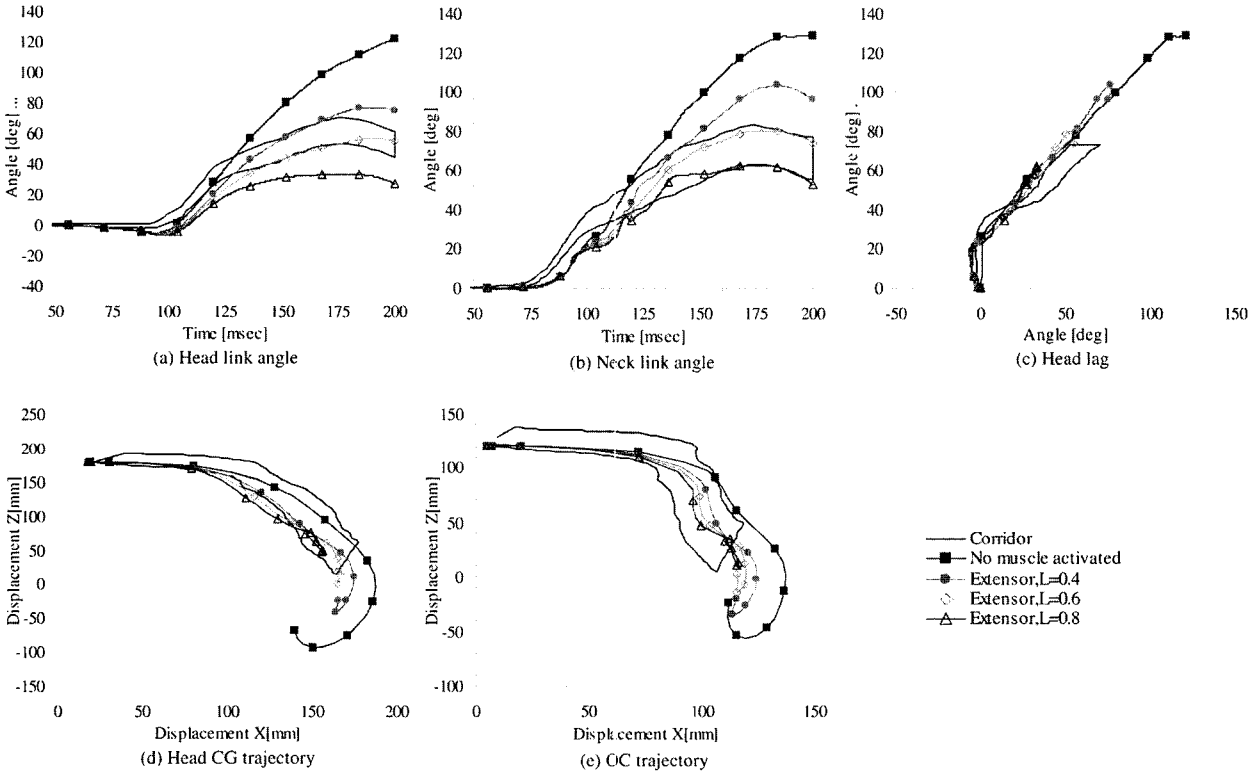

Figure 20. Comparison of head/neck kinematics between SIMon model simulation and NBDL test corridors: Effect of extensor muscle active state level, reflex time is fixed at 80 ms.

Table 8. Muscular variables in parametric simulation study for NBDL.

Variables	Ranges
Extensor muscle active level	0%, 40%, 60%, 80%
Reflex time	60 ms, 80 ms, 100 ms
Contractions	Extensor only, both extensor and flexor

the sled test(van der Horst, 1997), the reflex time and active state level of extensor muscles were chosen as variables for the parametric study in the simulation. Also the effects of co-contraction together with flexor muscles were investigated in the simulation. Table 7 shows the variables in a parametric simulation study for the NBDL 15G frontal sled test with their ranges.

Figure 20 shows the comparison of the head/neck kinematics between NBDL test corridors and simulation results with different active levels of the extensor

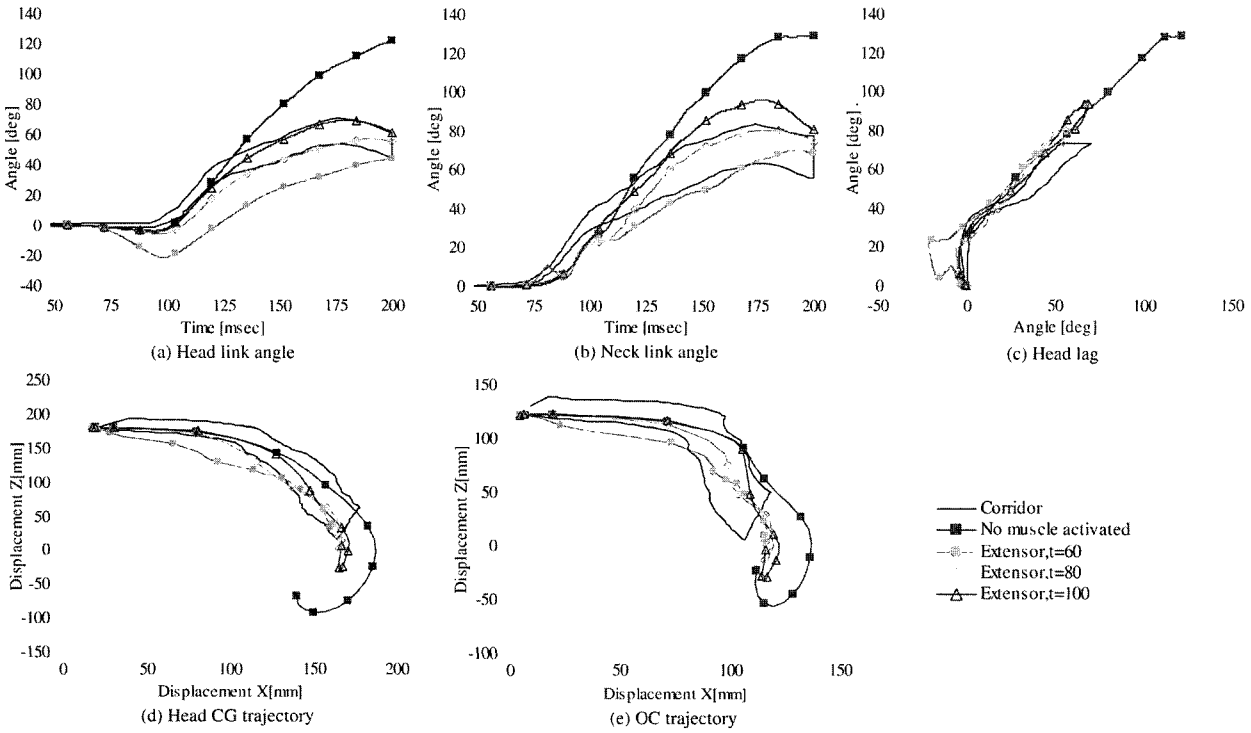

Figure 21. Comparison of head/neck kinematics between SIMon model simulation and NBDL test corridors: Effect of Reflex time, extensor muscle active state level is fixed at 60%.

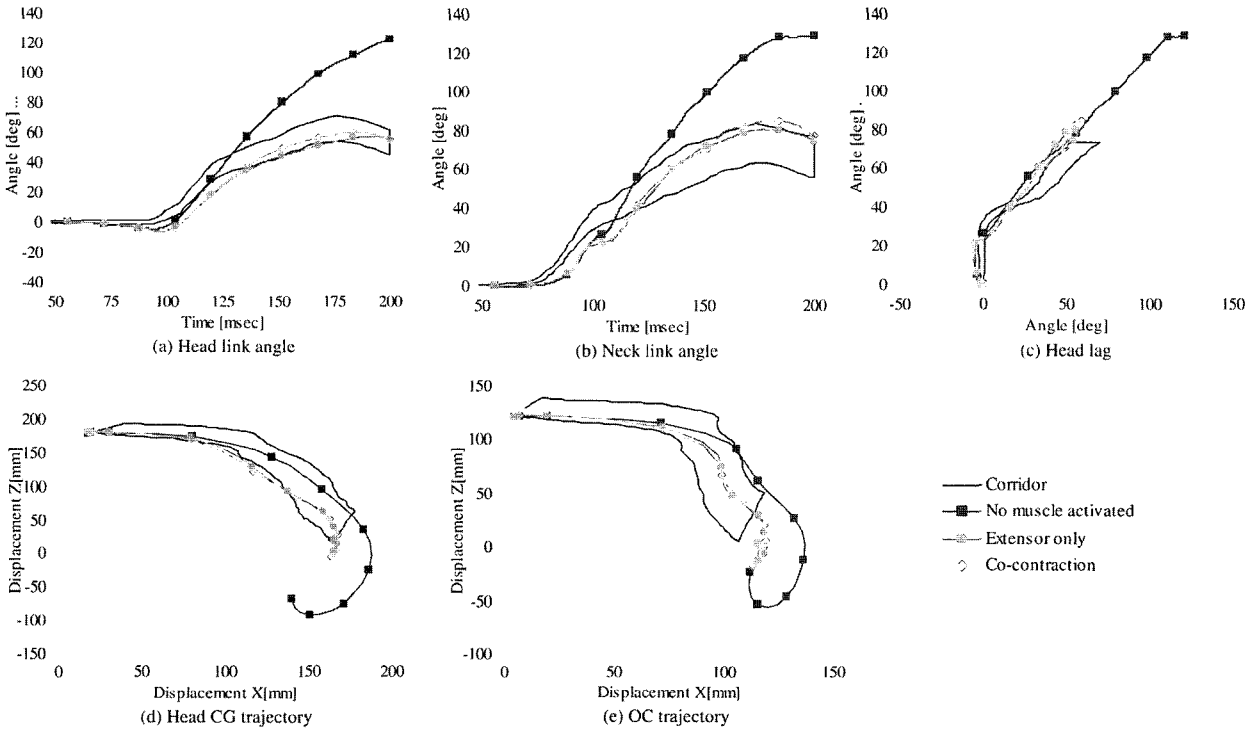

Figure 22. Comparison of head/neck kinematics between SIMon model simulation and NBDL test corridors: Effect of co-contraction, both extensor and flexor muscle active state level is fixed at 60% with reflex time at 80 ms.

muscles. Head and neck link angles in Figures 20(a) and (b) are expressed relatively to T1 rotation given in Figure 19(c). In this case, the reflex time was fixed at 80 ms and flexor muscles were not activated.

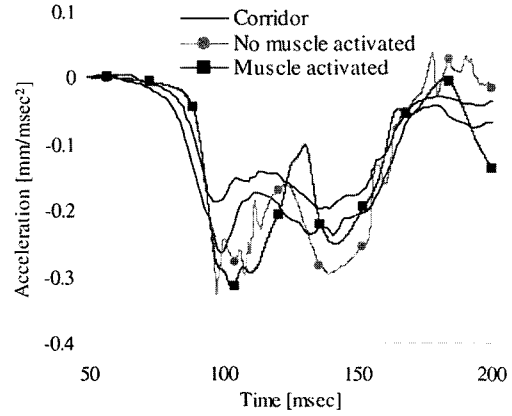

(a) Linear X acceleration of head CG

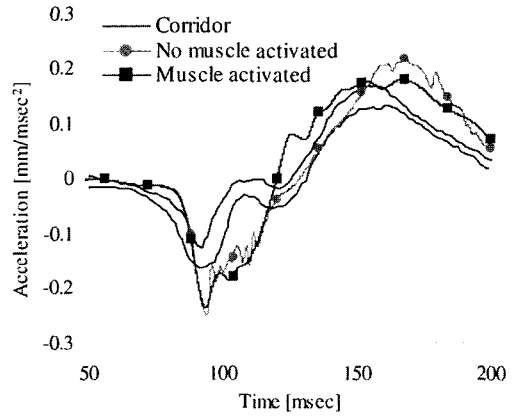

(b) Linear Z acceleration of head C.G

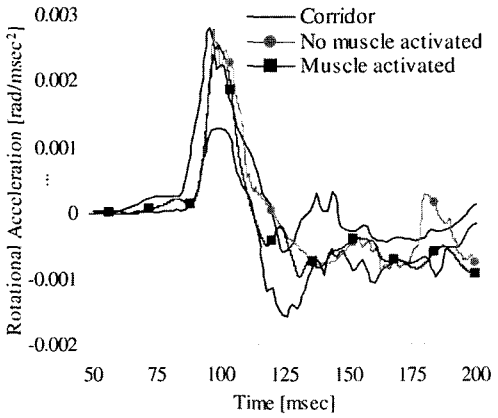

(c) Rotational Y acceleration of head CG

Figure 23. Comparison of head CG accelerations between SIMon model simulation and NBDL test corridors: 60% of active state level and 80 ms of reflex time of extensor muscles.

The simulation with 60% activation of extensor muscles correlates better than the other active state level conditions as shown in Figure 20.

Figure 21 shows the comparison of head/neck kinematics between NBDL test corridors and simulation results with different reflex time of extensor muscles. In this case, the active state level of extensor muscles was fixed at 60% and flexor muscles were not activated.

The simulation with 80 ms reflex time of extensor muscles correlates better than the other reflex time conditions as shown in Figure 21.

The simulated effects of co-contractions of agonist (extensor muscles) and antagonist (flexor muscles) is shown in Figure 22 by comparing with the head/neck kinematics from NBDL test corridors. In this case, the reflex time and active state level were fixed at 80 ms and 60%, respectively.

The simulation result shows no significant difference in head/neck kinematics between the case of agonist muscles contracted alone and the case of both agonist and antagonist muscles co-contracted as shown in Figure 22. The results of the parametric study shown in Figures 20

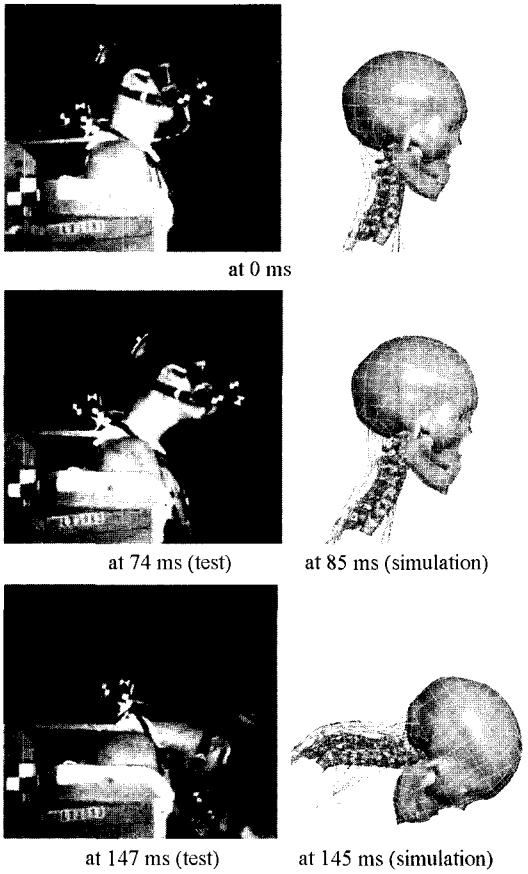

Figure 24. Pictures of head/neck response from NBDL 15G frontal sled test (Thunnissen, 1995) and simulations.

to 22 indicate that the most well correlating muscle conditions to NBDL 15G frontal sled volunteer test results are 80 ms of reflex time and 60% of extensor muscle active state level. It was not clear to make a selection from different contraction patterns, i.e. co-contraction or single contraction, since the results are quite similar to each other.

Figure 23 displays the comparison of head CG accelerations in translational (X and Z) and rotational (Y) directions with the above mentioned most well correlating muscle conditions together with the case of no muscles activated and Figure 24 shows the corresponding simulated head/neck response compared with the pictures of a volunteer (Experiment LX3983, Subject H00134) in NBDL 15G frontal sled test.

5. DISCUSSION AND CONCLUSION

In order to complete the proposing finite element human neck model, the followings are needed to be carried out in addition to the features of the model introduced in this paper.

More validations with whole cervical spine stiffness and strain rate effects: The lateral flexional and axial torsional response of whole cervical spine need to be investigated as well as its strain rate effect.

Soft tissue rupture modeling: The validation of failure prediction of inter-vertebral disc and ligament in various modes are under progress by adopting an appropriate modeling scheme using damageable elements with property degradation option.

Reconstruction of neck kinetics from measured dummy kinematics: Inverse dynamic approach would be employed to reconstruct the neck force and moment from the dummy kinematics measurement during the test procedure. The possible direct impact loading to neck such as a hit from deploying airbag could be handled by transposing the contact pressure into equivalent upper and lower neck loads. Appropriateness of proposing inverse dynamic approach would go through sufficient verification process.

New biomechanical injury criteria: The current neck injury criterion, Nij is based on kinetic information like force and moment acting on the interface junctions of neck. This Nij correlates the overall injury potentials upon the severity of applied neck loads. The anatomically precise finite element human neck model, proposed here as SIMon neck, furthermore facilitate the assessment of biomechanical injuries such as soft tissues damages and dislocation or sub-luxation of vertebral body and cervical zygapophysial joint with specific information of injury development locations.

ACKNOWLEDGEMENT–The authors express their appreciation to B. Myers, R. Nightingale, F. Pintar, and A. Wittek for the helpful comments on this work. This study was supported, in part, by Korean ministry of science and technology (Project No.: M10139080001-02B0808-00210).

REFERENCES

Bandak, F. A., and Eppinger, R. H. (1994). A three-dimensional finite element analysis of the human brain under combined rotational and translational accelerations. Internal report. *National Highway traffic Safety Administraion*, U.S.A.

Bandak, F. A. (1996). Biomechanics of impact traumatic brain injury. *Proceedings of the NATO-ASI on Crashworthiness of Transportation Systems: Structural Impact and Occupant Protection*, Troia, Portugal, 213–253.

Chancey, V. C., Van Ee, C. A. Nightingale, R. W., Camacho, D. L. and Myers, B. S. (2000). Understanding and minimizing error in cervical spine tensile testing. In NHTSA ed. *Injury Biomechanics Research: 28th International Workshop*, San Antonio, U.S.A.

Chazal, J. A., Tanguy, M. Bourges, G. Gaurel, G. Escande, M. Guillot and G. Vanneuville (1985). Biomechanical properties of spinal ligaments and a histological study of the supraspinal ligament in traction. *Journal of Biomechanics* **18, 3,** 167–176.

Choi, H. Y., Lee, I. H. and Haug, E. (1999). Advanced finite element modeling of the human body for occupant safety; H-Model for the next millennium. *Proceeding of 5th HanPam*, Seoul, Korea.

Claessens, M., Sauren, F. and Wismans J. (1997). Modeling of the human head under impact conditions: A parametric study. *SAE Paper No.* 973348.

Edwards, W. T. (1999). Mechanical properties of cervical spine tissues. *ISR Report*, Syracuse University, U.S.A.

ESI (2002). *PAM-CRASH SAFE V2002 Solver Notes Manual.* ESI Software.

Jager, M. K. J. de (1996). Mathematical head-neck models for acceleration impacts. *Ph.D thesis, University of Eindhoven*, Nederlands.

Lee, S. K. (2000). Current trend of crash and safety regulations. *J. KSAE* **22, 2,** 20–26.

Lee, I. H., Yoon, S. B., Lee, J. H. and Choi, H. Y. (2003). Development of finite element human models for crashworthiness simulation: Part I-50% male model. *KSAE Fall Conference Proc.*, Busan, Korea.

Moroney, S. P., Schultz, A. B., Miller, J. A. A. and Andersson, G. B. J. (1998). Load-displacement properties of lower cervical spine motion segments. *Journal of Biomechanics* **21, 9,** 769–779.

Myers, B. (2002). *Personal Communication.* Nov. at Jacksonville. U.S.A.

Myers, B. (2003). *Personal Communication.* March at Washinton D.C., U.S.A.

Nahum, A. M., Smith, R. and Ward, C. C. (1977). Intracranial pressure dynamics during head impact. *Proceedings of the 21st Stapp Car Crash Conference,* New Orleans, Louisiana, U.S.A., *SAE Paper No.* 770922.

Nightingale, R., Chancey, V., Luck, J., Tran, L., Ottaviano, D. and B. Myers, (2002). Accounting for Frame and Fixation Compliance in Cervical Spine Tensile Testing, In NHTSA ed. *Injury Biomechanics Research: 30th International Workshop,* Jacksonville, Florida, U.S.A.

Nightinglale, R. (2003). *Personal Communication.* March at Washington D.C., U.S.A.

Ono, K., Kaneoka, K., Hattori, S., Ujihashi, S., Takhounts, G. E., Haffner, M. and Eppinger, H. R. (2002). Cervical vertebral motions and biomechanical responses to direct loading of human head. *IRCOBI Conference,* Munich, Germany, 235–248.

Ono, Koshiro (1999). Relationship between localized spine deformation and cervical vertebral motions for low speed rear impacts using human volunteers. *IRCOBI Conference,* Spain, 149–164.

Panjabi, M. M., Crisco, J. J., Vasavada, A., Oda, T., Cholewicki, J., Nibu, K. and E. Shin (2001). Mechanical properties of the human cervical spine as shown by three-dimensional load-displacement curves. *SPINE* **26, 24,** 2692–2700.

Pintar, F. A. (1986). The biomechanics of spinal elements. *Ph.D Thesis,* Marquette University, U.S.A.

Pintar, F. A. (2003). Personal communication at 18th ESV Conference. Nagoya, Japan.

Robbin, D. H. (1983). Anthropometry of motor vehicle occupants. Vol. 2 Mid-sized male. *UMTRI report.,* U.S.A.

Stone, R. J. and J. A. Stone (2000). *Atlas of Skeletal Muscles.* 3rd Edition. McGraw-Hill. New York.

Szabo, T. J. and Walcher, J. B. (1996). Human subject kinematics and electromyographic activity during low speed rear impacts. Albuquerque, *Proceedings of the 40th STAPP Car Crash Conference,* New Mexico, U.S.A., *SAE Paper No.* 962432.

Thunnissen, J., Wismans, J., Ewing, C. L. and Thomas, D. J. (1995). Human volunteer head-neck response in frontal felxion: A new analysis. *Proceedings of the 39th STAPP Car Crash Conference,* San Diego, California, U.S.A., *SAE Paper No.* 952721.

Van der Horst, M. J. (1997). The influence of muscle activity on head-neck response during impact. *Proceedings of the 41st STAPP Car Crash Conference,* Lake Buena Vista, Florida, U.S.A., *SAE Paper No.* 973346.

Voo, L., Kumaresan, S., Pintar, F. A., Yoganandan, N. and Sances, Jr. A. (1996). Finite-element models of the human head. *Medical & Biological Eng. & Computing* **34, 5,** 375–381.

White, III A. A. and Panjabi, M. M. (1990). *Clinical Biomechanics of the Spine.* J. B. LIPPINCOTT COMPANY, 2nd Edition, New York.

Williams & Warwick, (1980). *GRAY's Anatomy,* 36th British Edition, W. B. Saunders Company.

Willinger, R., Kang, H. S. and Diaw, B. (1999). Three-dimensional human finite-element model validation against two experimental impacts. *Annals of Biomedical Eng.* **27,** 403–410.

Wismans, J., Oorschot, H. van and Woltring, H. J. (1986). Omni-directional human head-neck response. *Proceedings of the 30th STAPP Car Crash Conference,* San Diego, California, U.S.A., *SAE Paper No.* 861893.

Yoganandan, N., Kumaresan, S. and Pintar, F. A. (2001). Biomechanics of the cervical spine Part 2. Cervical spine soft tissue responses and biomechanical modeling. *Clinical Biomechanics* **16,** 1–27.

Wittek, A., Ono, K., Kajzer, J., Ortengren, R. and Inami, S. (2001). Analysis and comparison of reflex times and electromyograms of cervical muscles under impact loading using surface and fine-wire electrodes. *IEEE Trans. on Biomedical Eng.* **48,** 143–153.